

Short-Term Directional Variability of the Continuum Range in the Deep-Ocean Internal Wave Field

Melbourne G. Briscoe

Office of Naval Research, Arlington, Virginia

Abstract. A simple method (Zalkan, 1970) to examine the directionality of the internal wave field has been applied to temperature data at 1000 m depth from the IWEX trimooring (Briscoe, 1975). Results suggest the concept of a horizontally-isotropic deep-ocean internal wave field is not valid over 75-hour periods, but only over a longer time average. The estimated wavenumbers, for each frequency examined, lie along the calculated dispersion relation for modes 1-4.

1. Background

It is commonly argued that deep-ocean (> 500 m) internal waves are horizontally isotropic (i.e., no preferred direction of propagation), whereas upper-ocean (< 200 m) internal waves tend to occur in intermittent groups that propagate in specific directions. The original reference for the deep result was Garrett and Munk (1972), buttressed by Muller et al. (1978); recent results have only differed for the internal tidal frequencies. The seminal references for the upper-ocean result were the numerous papers of Sabinin and his coworkers e.g., Sabinin (1971, 1973) and the observations from FLIP reported originally, for example, by Zalkan (1970) and Pinkel (1975).

Part of the reason for the different views of the deep and upper ocean is simply that the observational techniques and the analysis methods have often been quite different in the two depth regimes, and to a certain extent the differing results have been therefore inevitable. For example, the deep experiments tend to be of long duration and are usually analyzed to yield the mean spectral properties. The upper ocean experiments tend to be quite short, often only a few days, and usually are analyzed in a way that emphasizes the time variability, for example wave packets and significant events.

However, it is possible to find many data that contradict the common view. Briscoe (1974) analyzed IWEX data (1000 m depth) in the same way that Zalkan (1970) looked at upper ocean data and found numerous instances where the deep-ocean internal wave field appeared to be time-varying and directional; those unpublished results are given here, with some extensions and a modern interpretation. Similarly, the detailed thermistor chain tows of Bell (1976) in the upper ocean show no significant horizontal anisotropy. Sabinin (personal communication, 1978) has commented that, contrary to his earlier work, he finds the Garrett-Munk spectrum to be quite reasonable as a description of the mean

state in the upper ocean. His conclusion is consistent with Roth et al. (1981) and unpublished work by Levine and coworkers (personal communication, 1999).

2. Introduction

The Internal Wave Experiment (IWEX) in 1973 was a deep-sea three-dimensional mooring array (current meters and temperature sensors) designed to act as an antenna for internal waves in the main thermocline. Briscoe (1975) describes the experiment and basic results; Muller et al. (1978) give the detailed analysis for the mean conditions

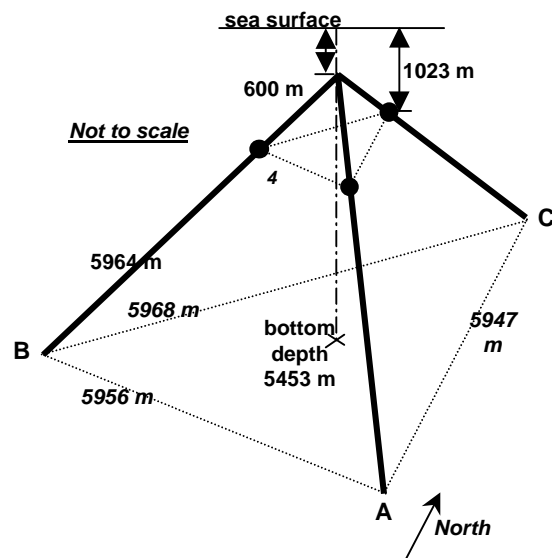


Figure 1. The IWEX Trimoor. The horizontal triangle of temperature sensors at 1023 m depth, separated 450 m, is the source of the data analyzed here. The location of the mooring was $27^{\circ}43.9' N$, $69^{\circ}50.95' W$, on the Hatteras Abyssal Plain south of Woods Hole and east of Scripps. See Briscoe (1975) for details.

over the 40-day experiment. Figure 1 shows the mooring array shape; instruments were distributed along the three legs of the mooring. Of note is the triangular horizontal triplets of instruments with horizontal spacings of a few meters to about a kilometer.

From the three temperature time-series at the 1000 m-level on the IWEX trimoor (~ 450 m horizontal separation) one may attempt to fit an incoming plane wave to the measured phase differences from the cross-spectra. The technique applied here is copied from *Zalkan* (1970) who argued for his data that a single plane wave of a single vertical mode was an adequate, perhaps even good, representation of the high-frequency internal wave field for short time intervals. The argument is not totally convincing, for one may always find a single “wave” that will “best fit” the phase differences, even if multiple waves, non-planar, from various directions are simultaneously present. *Zalkan* suggested that agreement between the estimated wave number, for a given frequency, and a theoretical wave number calculated from the dispersion relation for some mode, would support the argument. He showed (his Table III) such acceptable solutions and concluded that the relatively high-frequencies are well-fit by a single wave of the first mode. However, the low-frequencies were poorly fit by this approach.

Here I report a simple but illuminating attempt to apply those ideas to a fraction of the IWEX data set.

3. Method

Given three sensors, A-B-C, three possible phase differences for each frequency can be calculated from the three cross-spectral pairs; call the phases N_{AB} , N_{BC} , and N_{CA} . An incoming plane wave of wavenumber \mathbf{K} will project on the A-B-C sensor separations, \mathbf{X} , to yield phase differences:

$$N_{ij} = \mathbf{K} \cdot \mathbf{X}_{ij} = K_X X_{ij} + K_Y Y_{ij} \quad (1)$$

For the IWEX tri-mooring the sensors A and C were aligned south-north, respectively; B was west of the A-C line and completed an equilateral triangle of side L ; at the 1023 m depth $L = 450$ m.

Consequently,

$$-X_{AB} = X_{BC} = \frac{1}{2} L \ 3^{1/2}; \quad X_{AC} = 0 \quad (2a)$$

$$+Y_{BC} = Y_{AB} = \frac{1}{2} Y_{AC} = \frac{1}{2} L \quad (2b)$$

Therefore,

$$N_{AB} = -\frac{1}{2} 3^{1/2} L K_X + \frac{1}{2} L K_Y \quad (3a)$$

$$N_{BC} = +\frac{1}{2} 3^{1/2} L K_X + \frac{1}{2} L K_Y \quad (3b)$$

$$N_{AC} = L K_Y \quad (3c)$$

There are only two unknowns, K_X and K_Y , for the incoming plane wave, yet taking equations (3) two at a time yields three different estimates each for K_X and K_Y . Hence one writes, following *Zalkan*,

$$K_{RMS} = \left[\frac{1}{3} \left(\sum_{i=1}^3 K_X^{(i)^2} + \sum_{i=1}^3 K_Y^{(i)^2} \right) \right]^{1/2} \quad (4)$$

Similarly, the angle of incidence of the estimated plane wave is

$$\Theta_{RMS} = \arctan \left(\frac{\sum_{i=1}^3 K_Y^{(i)}}{\sum_{i=1}^3 K_X^{(i)}} \right) \quad (5)$$

Hence, for each frequency f , one may obtain $K_{RMS}(f)$, and $\Theta_{RMS}(f)$.

4. Data

I broke up the three approximately 40-day temperature records into 13 non-overlapping pieces of 75 hours each (length chosen to give minimal spectral leakage from tidal and inertial bands). Coherences and phases were calculated by smoothing over 14 frequency bands, giving 28 degrees of freedom. The lowest-frequency estimate was consequently $14/75 = 0.187$ cph. Because the coherences dropped with increasing frequency, the phase estimates were stable only for frequencies less than about 1.7 cph. Hence, 1.68 cph was the highest frequency considered.

In a program on a PC the relations (4) and (5) were calculated, using the phase data from the coherence/phase estimates. The frequencies involved were 0.187, 0.373, 0.560, 0.747, 0.933, 1.120, 1.307, 1.493, and 1.680 cph.

5. Results

Figure 2 shows a polar plot (north up) of the $K_{RMS}(f)$, and $\Theta_{RMS}(f)$ results for each of the 9 frequencies and for each of the 13 data pieces. The solid circles are scale-circles having wavenumbers equivalent to 20, 10, 5, 2, 1, and 0.5 km, stating from the origin. The radial scale is logarithmic in km^{-1} . Each $K_{RMS} - \Theta_{RMS}$ solution is plotted in the same color for its time segment from which it was obtained, regardless of which frequency it applies to. The plotted direction is the direction from which the wave is incident.

Figure 2 should be viewed as a kind of zoom view of what an average internal wave field looks like: overall, there is no particular directionality, but at any moment for any frequency there is something more distinct happening.

Figure 3 is the same as Figure 2 except only the 9 $K_{RMS} - \Theta_{RMS}$ solutions for the first 75-hour time segment are shown. Here, the waves are clearly incident from either the southwest or the northeast. Other time segments show either no pattern, or their own pattern. For example, time segment 4 (yellow) is mostly propagation from the northwest, and segment 8 is mostly from the southwest.

Figure 4 presents the same data as in Figure 2 but sorted by frequencies rather than time pieces. Again, each $K_{RMS} -$

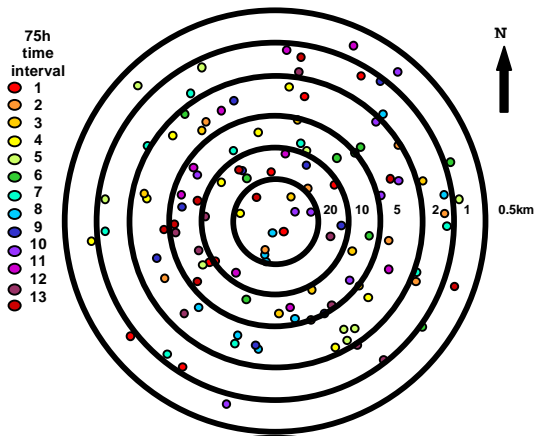


Figure 2. Polar plot of incident wave numbers based on single plane-wave analysis of the temperature coherences. Plot is direction of wave travel (North = \uparrow) versus log wavenumber, given as wavelength. Each color refers to one of 13 consecutive 75-hour time periods. For each time period there are 9 frequencies plotted here. No preferred direction of propagation exists over the total 40-day period.

I_{RMS} solution is plotted in the same color for its frequency, regardless of which time segment it came from.

Now some trends are clearer, but the results are mostly just indicative of the dispersion relations for an internal wave field. That is, in a modal framework, a given frequency should have some preferred wavenumbers. This is quickly seen with the red-yellow (lower) frequencies having smaller preferred wave numbers, and the green-blue (higher) frequencies having larger preferred wavenumbers. Figure 5 quantifies this: the average K_{RMS} for each frequency is

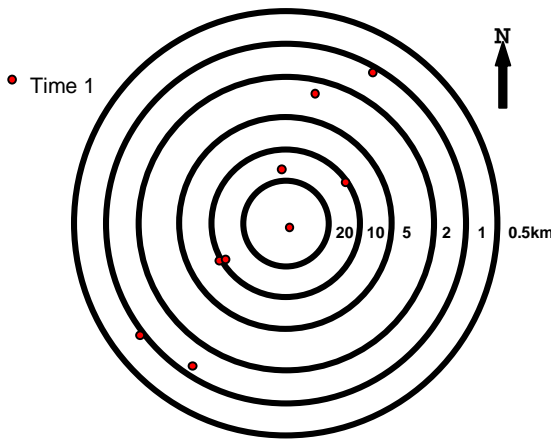


Figure 3. Same as Figure 2, but only the wavenumbers for nine frequencies from the first 75-hour time period are shown, to illustrate strong directionality for all frequencies during that time period.

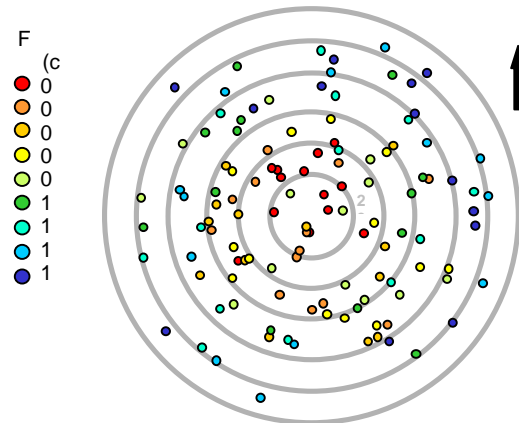


Figure 4. Same as Figure 2, but no each color refers to one of 9 frequency bands. For each frequency band there are 13 consecutive time periods plotted here.

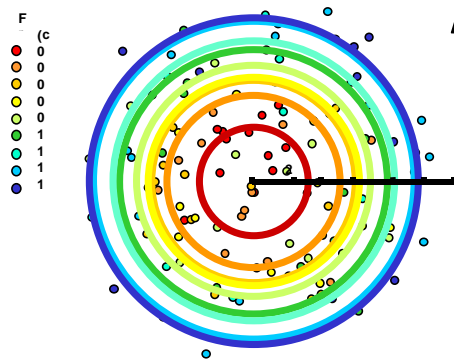


Figure 5. Same as Figure 4, but colored circles are added at the wavenumber magnitude that is the average for each frequency.

plotted as a circle of the same color as that in which the frequencies are coded. (higher) frequencies having larger preferred wavenumbers. Figure 5 quantifies this: the average K_{RMS} for each frequency is plotted as a circle of the same color as that in which the frequencies are coded.

Figure 6 compares the empirical dispersion relation of Figure 5 (the solid black dots are the average K_{RMS} for each frequency) to the theoretical dispersion relations (for the first 4 modes) calculated from the mean buoyancy frequency profile for the IWEX site. The error bars are ± 1 standard deviation (based on the 13 pieces). The K_{RMS} seems to follow the fourth mode for the lower frequencies, and the third mode for the higher frequencies, which is approximately consistent with a Garrett-Munk j_s of 3. The transition occurs at about the wavenumber-frequency of the

Eckart resonance for the IWEX buoyancy frequency (Eckart, 1969; Katz and Briscoe, 1979).

6. Discussion

The same caveats apply here as in Zalkan's work: (1) it is unlikely *a priori* that a single plane wave can account for the observed coherences; (2) the technique cannot distinguish between one plane wave and several in different directions, nor between one and several of different vertical modes.

Nevertheless, the results are consistent with a modal-model in the sense that Zalkan found consistency.

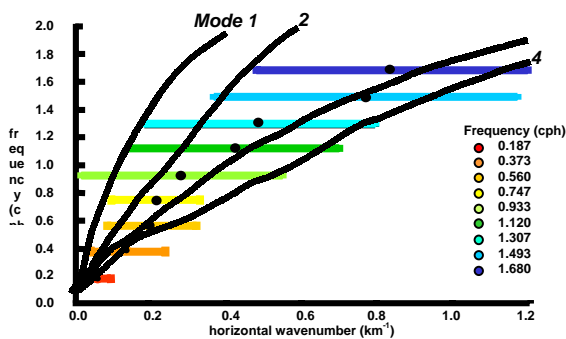


Figure 6. Empirical dispersion curve for the data set, for each of 9 frequencies, versus the average wavenumber from Figure 5. Error bars on wavenumber are ± 1 standard deviation over the 13-piece average. The solid black lines are the calculated dispersion curves for the local mean buoyancy frequency, for the first four modes.

This does not mean that only one mode is present (at each frequency), but rather that during each time segment, only a small number of modes (and lower modes) dominates. Were it otherwise, the estimated wavenumbers for each frequency would not fall so neatly along the low-mode dispersion curves.

Directionality is evident in these 75-hour time periods, but no pattern is obvious from one time period to the next. Thus, this analysis is consistent with internal wave sources being distributed in time and space and arriving at any one point from a variety of directions, but not from all directions at any one time.

Some internal consistency checks of the analysis are possible. When one examines a scatter plot of N_{AB} versus $N_{BC} + N_{CA}$, most of the points are consistent with the diagonal line that represents perfection. This simplest-possible consistency check works fairly well, and suggests the phases observed are meaningful and interpretable as being due to a simple modal/wave system at each frequency for each time segment.

This analysis means a non-directional internal wave field (at the higher frequencies, in the deep ocean) is true in the

average over 40 days but is not certain at all frequencies for all 3-day periods. Additionally, during the shorter time intervals, the incident internal wave field is composed of a fairly simple modal structure.

From the point of view of using an instantaneous description of the internal wave field as an input to acoustic propagation applications, these data suggest it would be better to include this directionality than to ignore it. The original *Garrett-Munk* (1972) argument for an isotropic spectrum is true only in the mean; acoustic propagation does not see the mean state.

Acknowledgments. I thank my quarter-century colleague in IWEX, Peter Muller, for a continuing series of stimulating discussions on internal waves. This work was originally performed at Woods Hole Oceanographic Institution, but was written up while at the Office of Naval Research under the Research Opportunities for Program Officers (ROPO) program.

References

- Bell, T. H., Jr., The structure of internal wave spectra as determined from towed thermistor chain measurements, *J. Geophys. Res.*, *81*, 3709-3714, 1976.
- Briscoe, M. G., Directional variability by plane wave analysis, in *Status Report on IWEX - June 1974*, edited by M. G. Briscoe, Woods Hole Oceanographic Institution, 1974. [copy of article available from author]
- Briscoe, M. G., Preliminary results from the trimoored internal wave experiment (IWEX), *J. Geophys. Res.*, *80*, 3872-3884, 1975.
- Eckart, C., Internal waves in the ocean, *Phys. Fluids*, *4*, 791-799, 1961.
- Garrett, C. J. R., and W. H. Munk, Space-time scales of internal waves, *Geophys. Fluid Dyn.*, *2*, 225-264, 1972.
- Katz, E.J., and M.G. Briscoe, Vertical coherence of the internal wavefield from towed sensors, *J. Phys. Oceanogr.*, *9*, 518-530, 1979.
- Muller, P., D. J. Olbers, and J. Willebrand, The IWEX spectrum, *J. Geophys. Res.*, *83*, 479-500, 1978.
- Pinkel, R., Upper ocean internal wave observations from FLIP, *J. Geophys. Res.*, *80*, 3892-3910, 1975.
- Roth, M.W., M.G. Briscoe, and C.H. McComas, Internal waves in the upper ocean, *J. Phys. Oceanogr.*, *11*, 1234-1247, 1981.
- Sabinin, K. D., Measurement of the parameters of internal waves by means of a moving, spatially-separated system of sensors, *Izv., Atm. Oc. Physics*, *7*, 379-381, 1971.
- Sabinin, K. D., Certain features of short-period internal waves in the ocean, *Izv., Atm. Oc. Physics*, *9*, 32-36, 1973.
- Zalkan, R. L., High-frequency internal waves in the Pacific Ocean, *Deep-Sea Res.*, *17*, 91-108, 1970.